

RESEARCH ARTICLE

10.1002/2016JA023417

Key Points:

- LSTIDs were detected in both Northern and Southern Hemispheres over the American sector during the geomagnetic storm on 17–18 March 2015
- LSTIDs in South and North Hemispheres with different propagation direction during the main phase of magnetic storm
- The observed propagation forms suggest asymmetric/symmetric auroral current activity between the northern and southern polar regions

Supporting Information:

- Supporting Information S1
- Movie S1
- Movie S2
- Movie S3
- Movie S4

Correspondence to:

C. A. O. B. Figueiredo,
cosme.figueiredo@inpe.br

Citation:

Figueiredo, C. A. O. B., C. M. Wrasse, H. Takahashi, Y. Otsuka, K. Shiokawa, and D. Barros (2017), Large-scale traveling ionospheric disturbances observed by GPS dTEC maps over North and South America on Saint Patrick's Day storm in 2015, *J. Geophys. Res. Space Physics*, 122, 4755–4763, doi:10.1002/2016JA023417.

Received 31 AUG 2016

Accepted 5 APR 2017

Accepted article online 10 APR 2017

Published online 25 APR 2017

Large-scale traveling ionospheric disturbances observed by GPS dTEC maps over North and South America on Saint Patrick's Day storm in 2015

C. A. O. B. Figueiredo¹ , C. M. Wrasse¹ , H. Takahashi¹ , Y. Otsuka², K. Shiokawa² , and D. Barros¹

¹Instituto Nacional de Pesquisas Espaciais, São José dos Campos, Brazil, ²Institute for Space-Earth Environmental Research, Nagoya University, Nagoya, Japan

Abstract Large-scale traveling ionospheric disturbances (LSTIDs) were detected in both Northern and Southern Hemispheres over American sector during the geomagnetic storm on 17–18 March 2015, also known as the Saint Patrick's Day storm. Detrended total electronic content (dTEC) maps were made using dense GNSS network receiver data. The retrieved LSTIDs showed wavelengths of 1000 to 2000 km, phase velocity of ~300–1000 m/s, and period of ~30–50 min. Among them, three couples of LSTIDs were observed propagating from the polar regions to low latitudes. Two wave events observed in daytime showed the propagation direction of southwest in the Northern Hemisphere and northeast in the Southern Hemisphere, which means an asymmetric propagation against the geographic equator. The other wave event observed during the evening hour showed symmetric propagation direction, i.e., southwest in the Northern Hemisphere and northwest in the Southern Hemisphere, whereas their wavelength and phase velocity are significantly different between NH and SH. These observations indicate that the two groups of LSTID have different propagation conditions from polar to low-latitude regions. The observed asymmetric/symmetric propagation forms suggest asymmetric/symmetric auroral current activity between the northern and southern polar regions.

1. Introduction

The observations of large-scale traveling ionospheric disturbances (LSTIDs) have been widely studied [Pradipta *et al.*, 2016; Song *et al.*, 2012; Valladares *et al.*, 2009; Tsugawa *et al.*, 2003, 2004, 2006; Afraimovich *et al.*, 2000]. LSTIDs are ionospheric signature of atmospheric gravity waves. These waves are generated by Joule heating and Lorentz force produced from intensified auroral electrojet and/or intense particle precipitation in the auroral and subauroral regions during the geomagnetic storms [Hunsucker, 1982]. Since LSTIDs propagate longitudinally and latitudinally in a global scale, they provide information on the energy and momentum transports from the high to low latitudes.

Ground-based network of GNSS receivers is a powerful tool to monitor oscillations over long distances (e.g., LSTIDs, MSTIDs). Using two-dimensional maps of detrended total electron content (hereafter dTEC), it is possible to extract the parameters of LSTIDs. Saito *et al.* [1998] built two-dimensional dTEC maps using TEC data from more than 1000 GPS receivers in Japan. They showed temporal and spatial variations of the medium-scale traveling ionospheric disturbances (MSTID).

Afraimovich *et al.* [2000] studied propagation of LSTIDs in the North American sector, covering a large area (30° to 70°N and 60° to 160°W). They observed that LSTIDs propagated to southwest. Following the same way, Nicolls *et al.* [2004] investigated the magnetic storm 1–2 October 2002 and found that a LSTID propagated toward the equator with a phase speed of 600 m/s. Afraimovich and Voeykov [2004] and Afraimovich *et al.* [2006] have studied the large magnetic storm event on 30 October 2003, where they found LSTIDs propagating southwestward. The same magnetic storm of 30 October 2003 was also studied by Ding *et al.* [2007]. They reported three LSTIDs propagating southwestward with the phase velocity between 270 and 740 m/s and period of 1 to 2 h. From the observed wave characteristics, they concluded that the westward auroral electrojet was a possible source of LSTIDs.

Tsugawa *et al.* [2003, 2004] performed a statistical analysis of the LSTIDs propagation characteristics using the Japanese network of GPS receivers and found a correlation of LSTIDs with the geomagnetic activity *Kp* index. Statistical study of LSTIDs, observed over North America (25° and 55°N) during the magnetic storms between

the years 2003 and 2005, has been carried out by *Ding et al.* [2008]. They showed that most of LSTIDs are solitary waves and occur mostly during the day, and the mean values of the period, phase velocity, and azimuth are 1.8 h, 300 m/s, and southwest, respectively. Furthermore, *Song et al.* [2012] presented that the direction of propagation depends on the latitude, i.e., in the low latitudes LSTIDs are deflected westward in the Northern Hemisphere. The average phase velocities are different in longitudes; North American sector (422 ± 36 m/s), Asian (527 ± 21 m/s), and the European sector (381 ± 69 m/s). They further pointed out that high phase velocity of LSTIDs is common in the low latitudes because of a lower amount of ion drag. During the last decade, observations of LSTID have been carried out by GNSS network mainly in the Northern Hemisphere (hereafter as NH). Whereas, few observation has been made in the Southern Hemisphere (hereafter as SH).

Shiokawa et al. [2005] observed an equatorward propagating LSTID at the conjugate points in Japan and Australia by using airglow imagers. They found a phase difference between the two waves of ~ 20 min and concluded that they were generated in the auroral regions and propagated equatorward independently without electromagnetic coupling. *Tsugawa et al.* [2006] studied LSTIDs at the geomagnetic conjugate points using Japanese GNSS networks and several receivers in Australia. They found five events of simultaneous observation of LSTID, reaching the same conclusions of *Shiokawa et al.* [2005].

In the American sector, *Valladares et al.* [2009] observed LSTIDs propagating equatorward and found that the phase velocity in the Northern Hemisphere (700 m/s) was higher than that in SH (550 m/s). *Pradipta et al.* [2016] characterized the interhemispheric propagation of auroral origin LSTIDs and found that the phase velocity in NH (1032 ± 353 m/s) was higher than that in SH (654 ± 40 m/s). They further observed an intensification of the LSTID amplitude around geomagnetic equator.

These previous works on LSTID during the magnetic storm conditions indicate that propagation of the waves launched from the NH and SH auroral regions seems to have an independent way of propagation each other and no effect of the electromagnetic coupling. Further, it seems that there is no consensus on the propagation direction, symmetric (southwestward direction in NH and northwestward in SH) or antisymmetric (southwestward direction in NH and north-northeastward direction in SH) against the geographic equator. Few simultaneous observations of LSTID from NH and SH make it difficult to get a conclusive idea on the wave characteristics and physical processes to explain them. Further observational evidences are necessary to extend our present knowledge on the LSTID.

Several LSTIDs were observed simultaneously in both the North American and South American sectors during the geomagnetic storm on 17 March 2015. The *Dst* index reached -223 nT and strong auroral activities were observed in both of the auroral ovals. A detailed account of the geomagnetic storm and its effects in the ionosphere has been reported by *Astafyeva et al.* [2015]. In the present work detrended TEC maps (dTEC) were obtained, which clearly showed wave propagating from the high latitudes to the equator during the period of 14:00 to 23:30 UT. Wave characteristics were calculated from the LSTIDs observed in NH and SH, i.e., horizontal wavelength, period, phase velocity, and propagation directions and compared them, in order to discuss the direction of propagation and phase velocity associated with symmetry/asymmetry at auroral region.

2. Observation and Data Analysis

In order to carry out a study of LSTIDs, it is necessary to detrend the observed TEC, so that small amplitude of TEC oscillations can be retrieved. In the present study, we calculate the perturbation components of TEC (dTEC) from $TEC(t)$ subtracting the TEC trend obtained from a 1 h running average for each couple of a ground receiver and GNSS satellite.

$$dTEC(t) = VTEC(t) - \overline{VTEC}(t \pm 30 \text{ min}).$$

Each GNSS dual-frequency receiver ($f_1 = 1.57542$ and $f_2 = 1.22769$ GHz, L band frequency) provides data with carrier phase and pseudo-range measurements every 30 s. The slant TEC (STEC) is calculated from the phase lag along the signal path between the satellite and the GNSS receiver using the following equation [*Mannucci et al.*, 1999]:

$$STEC = \frac{1}{40.3} \frac{f_1^2 f_2^2}{f_1^2 - f_2^2} [(L_1 - L_2) - (\lambda_1 n_1 - \lambda_2 n_2) + b_r + b_s],$$

where L_1 and L_2 are the recorded carrier phase (converted to distance units), λ is the wavelength of the radio wave, n_1 and n_2 are ambiguities of an integer cycle, and b_r and b_s are instrumental bias of the receiver and satellite couple, respectively. The present study is focused on perturbation component of TEC caused by LSTIDs; thus, we used the same approach of *Tsugawa et al.* [2006, 2007], which ignores the phase ambiguity and satellite and receiver biases. The vertical TEC (VTEC) can be obtained from the slant TEC and the satellite zenith angle projected, at the ionospheric pierce point, at 300 km:

$$VTEC = \cos \chi STEC,$$

where χ is the satellite zenith angle at the thin shell ionosphere located at the F region peak height (300 km). The zenith angle adopted for TEC calculation is smaller than 60° , i.e., elevation angle greater than 30° are used in calculation.

In the present work, we classified spatial and temporal variation of dTEC as a LSTID if the following criteria are satisfied: amplitude of oscillation larger than 0.1 TECU, horizontal wavelength greater than 1000 km, period greater than 30 min, horizontal phase velocity between ~ 300 and 1000 m/s [e.g., *Hunsucker, 1982; Hocke and Schlegel, 1996*].

The dTEC maps in Southern Hemisphere have a spatial resolution of $1 \times 1^\circ$ in latitude and longitude (spatial resolution of $0.2 \times 0.2^\circ$ smoothed by 5×5 elements). The grid is defined according to the spatial distribution of ionospheric pierce points (IPPs) (for IPP map over South America, see Figure 1b of *Takahashi et al.* [2016]) in order to observe oscillation with wavelength more than 150 km. Whereas the spatial resolution in the Northern Hemisphere is $0.75 \times 0.75^\circ$ in latitude and longitude (resolution of $0.15^\circ \times 0.15^\circ$ smoothed by 5×5 elements), this grid size is smaller than that in the Southern Hemisphere because the GNSS network's coverage is denser in North America. The dTEC value for each spatial resolution is an average of all pair receiver-satellite paths that cross the smoothing area at the IPPs for each 30 s for both hemispheres [e.g., *Tsugawa et al., 2006*].

The GNSS network used in this work consists of approximately 140 receivers in the Southern Hemisphere provided by Rede Brasileira de Monitoramento Contínuo (RBMC) and Red Argentina de Monitoreo Satelital Continuo (RAMSAC) Networks, and 2700 receivers in the Northern Hemisphere provided by International GNSS Service (IGS), Continuously Operating Reference Station (CORS), Scripps Orbit and Permanent Array Center (SOPAC) and University NAVSTAR Consortium (UNAVCO) networks. *Takahashi et al.* [2016] (see Figure 1a of *Takahashi et al.* [2016]) described in details the ground-based GNSS network in Southern Hemisphere, while *Tsugawa et al.* [2007] (see Figure 1 of *Tsugawa et al.* [2007]) showed the same network for Northern Hemisphere.

3. Results

Figure 1 shows the LSTIDs observed in both hemispheres over the American sector during the initial stage of the storm main phase on the St. Patrick's Day, 17 March 2015. Using a sequence of dTEC maps, we could observe four fronts LSTIDs: two in each hemisphere. In North America, Figures 1a and 1b show two dTEC maps with 20 min interval between 18:10 and 18:30 UT where it is possible to recognize two crests of LSTID propagating toward the southwest with a large distance between them and the estimated horizontal phase velocity of -529 ± 88 m/s. On the other hand, Figures 1c and 1d show dTEC maps of South America with 20 min interval between 16:00 and 16:20 UT. It is possible to see an LSTIDs feature in Argentina region, around 35°S (red region) propagating north-northeastward of Brazil, with a horizontal phase velocity of 611 ± 69 m/s. Two animations of Figures 1a/1b and Figures 1c/1d with a time resolution of 10 min and 30 s, respectively, are available through the supporting information related to this paper (see Movies S1 and S2). The color codes are in accordance with the disturbance signal, from red (positive) to black (negative).

In order to highlight the LSTIDs seen on Figures 1c and 1d in the Southern Hemisphere, a latitude-time cross section was made using keogram technique, which is shown in Figure 2. Keogram is made by taking a diagonal cross section starting at (10°S ; 40°W) and ending at (40°S ; 65°W) for each processed dTEC map image, and then taking the cross sections to create a time series (time resolution of 1 min) showing the

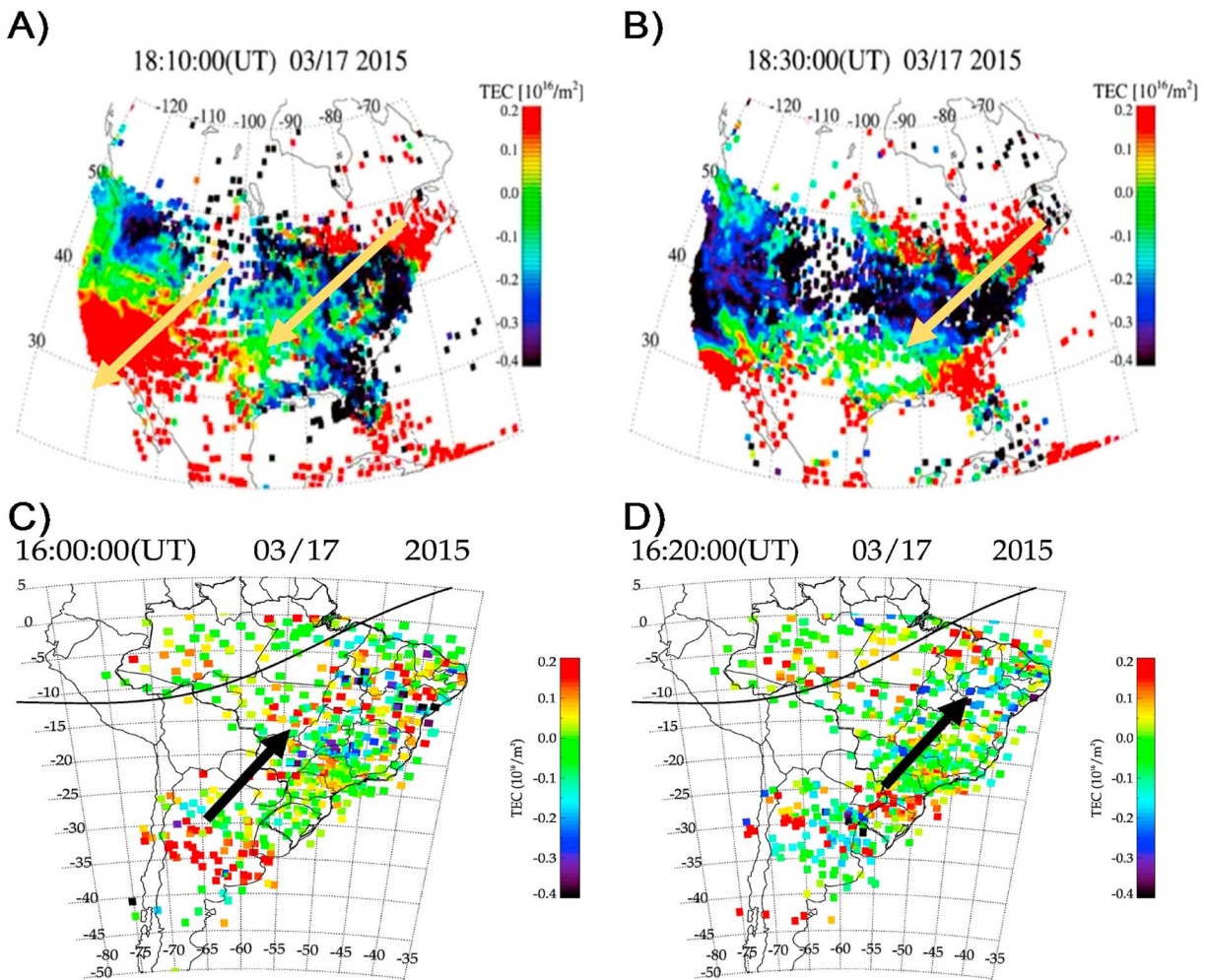


Figure 1. The dTEC maps for (a, b) Northern and (c, d) Southern Hemispheres observed during the period of 18:10–18:30 UT and 16:00–16:20 UT, respectively. Figures 1a and 1b show an LSTID propagating southwestward while Figures 1c and 1d show another LSTID propagating toward north-northeast. The arrows indicate the propagation directions. The black continuous line in Figures 1c and 1d is the geomagnetic equator.

variation of latitudinal component [e.g., Sobral et al., 2001; Saito et al., 2007; Taylor et al., 2009; Narayanan et al., 2014]. This diagonal cut was chosen in order to minimize the data gap. It is straightforward to identify three LSTIDs fronts propagating from pole to equator, the first one between 14:30 and 15:30 UT, the second one from 16:00 to 17:00 UT, and the third one from 18:30 to 19:00 UT, all of them propagating

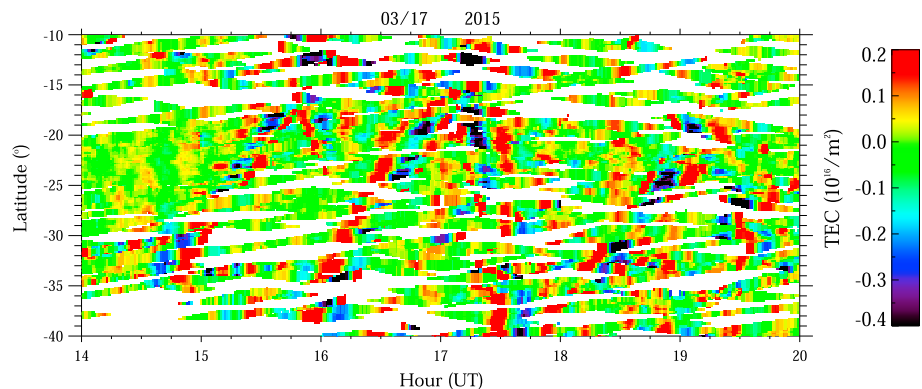


Figure 2. Latitude-time cross-section keogram of dTEC image over the South America from 10°S to 40°S, between 14:00 and 20:00 UT. The figure presents the latitudinal variation of dTEC along a diagonal cut from (10°S, 40°W) to (40°S, 65°W).

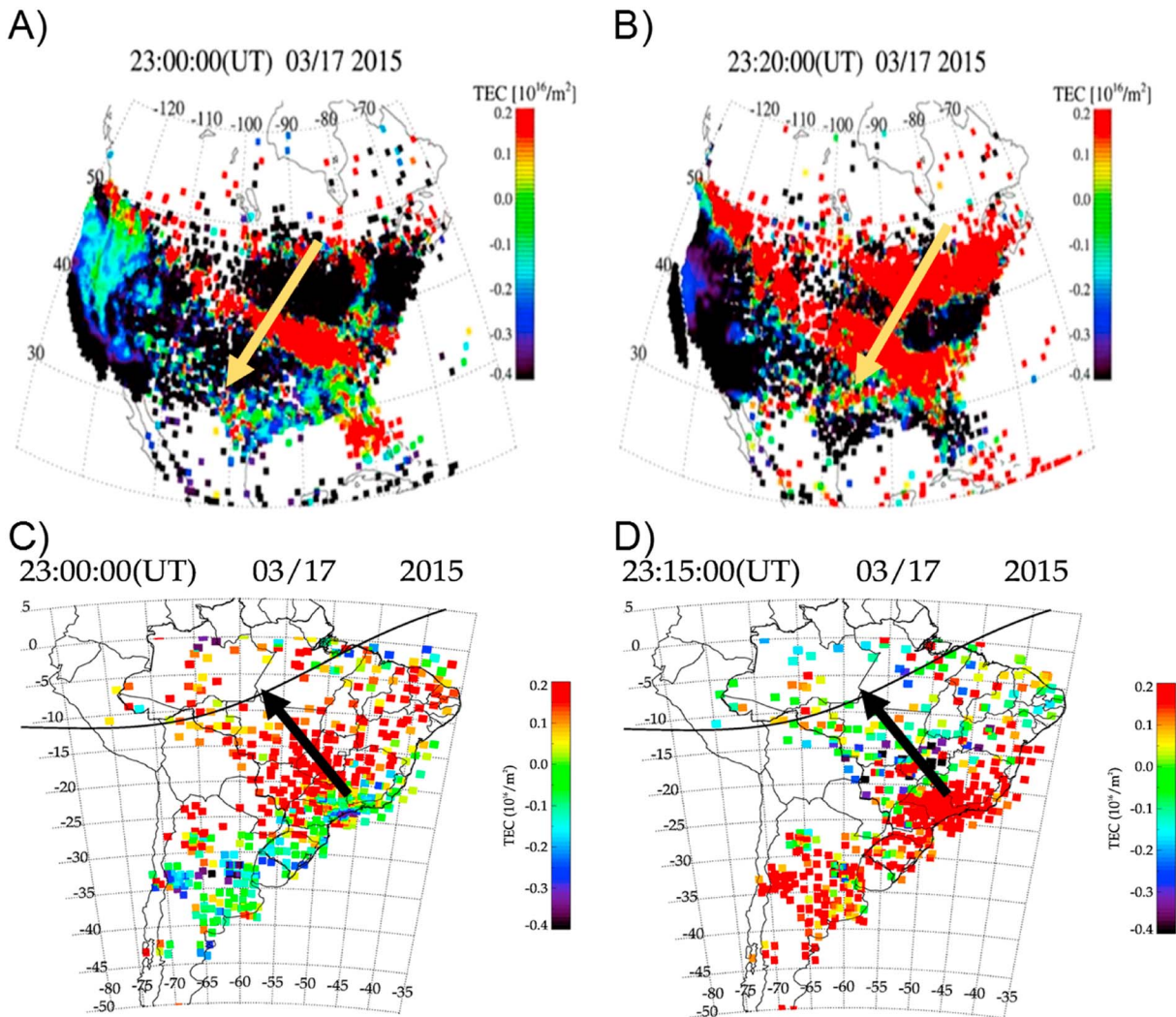


Figure 3. The dTEC maps for (a, b) Northern and (c, d) Southern Hemispheres observed during the period of 23:00–23:20 UT on 17 March 2015. These images show LSTIDs almost simultaneously propagating equatorward. Figures 3a and 3b show an LSTID propagating southwestward, while in Figures 3c and 3d LSTID propagates northeastward. The black continuous line is the magnetic equator and the arrows indicate the propagation direction of LSTID.

equatorward. The LSTID observed between 16:00 and 17:00 UT is the same as that presented in Figures 1c and 1d. On the other hand, we can notice that there are wave fronts propagating poleward, opposite to those presented above, at 15:30, 17:15, and 19:00 UT in Figure 2. We calculated the phase velocities and periods and found 1140 ± 160 m/s (29 ± 6 min), 1496 ± 170 m/s (32 ± 3 min), and 595 ± 14 m/s (24 ± 4 min), respectively. According to Hunsucker [1982] and Hocke and Schlegel [1996], the wave observed at 19:00 UT can be classified as LSTID and the others events do not fit the criteria of LSTIDs. Due to the lack of data between 0 and 10°S, we could not identify whether these waves came from the equator or even from the Northern Hemisphere [e.g., Pradipta et al., 2016].

Figure 3 presents four snapshots of dTEC maps for NH (Figures 3a and 3b) and SH (Figures 3c and 3d) during the main phase of the geomagnetic storm on 17 March 2015. In NH there is an LSTID propagating to Southwest, indicated by the arrows. The estimated horizontal phase velocity was 291 ± 59 m/s. Meanwhile, Figures 3c and 3d show a LSTID in Southern Hemisphere propagating to the northwest (as indicated by the arrows), and a horizontal phase velocity of 1070 ± 84 m/s. An animation of Figures 3a and 3b with 10 min time resolution and another animation with resolution of 30 s for Figures 3c and 3d are also available through the supporting information associated with this paper (see Movies S3 and S4).

4. Discussion

During the geomagnetic storm that occurred on 17 March 2015, several LSTID events were observed in the longitudinal zone of the American sector. As shown in Figures 2 and 3, four LSTIDs were propagating equatorward from the SH high latitudes. On the other hand, in the NH, three LSTIDs were propagating southwestward. The characteristics of the observed LSTIDs are summarized in Table 1. Each wave event was designated as SH1, NH1, and so on. LSTIDs were grouped according to the time of occurrence in each hemisphere. In the present paper, we do not intend to discuss conjugate propagation of LSTIDs, because of the large latitudinal differences of the observation area, in the NH (middle to high latitudes) and SH (equatorial to middle latitudes). It seems that the LSTIDs events SH1 and NH1 (14:00–14:30 UT), and SH3 and NH2 (18:00–18:30 UT) have same characteristics, i.e., wavelength of ~ 1000 km and phase speed of 500–700 m/s. Their propagation directions were different, southwestward in the NH and northeastward in the SH, which called our attention and will be discussed in the next section. The wave observed at 35°S is approximately 3000 km away from the southern auroral oval region. If we consider a phase velocity of ~ 700 m/s, it takes around 1.2 h for the wave to reach the latitude of 35°S . On the other hand, the wave event was observed around 50°N , much closer to the northern auroral oval (~ 1000 km) which takes around 30 min, with a phase velocity of ~ 500 m/s for the wave to reach that region. Therefore, the LSTIDs were launched at the auroral ovals at different moments and under different geomagnetic conditions. A similar wave event to SH2, at 16:00 UT, was not observed in the NH.

The wave events SH4 and NH3 occurred at 23:00 UT, and the amplitude of oscillation was stronger ($d\text{TEC} > 0.2$ TECU) than the previous ones. However, it should be pointed out that the phase velocities of LSTIDs are significantly different between the NH and SH waves. A faster phase velocity was observed in the SH. In addition, the propagation directions were also different, northwest in SH and southwest in NH.

Different propagation characteristics of LSTID during the main phase of geomagnetic storm have been previously studied by Tsugawa *et al.* [2006] and Valladares *et al.* [2009]. Tsugawa *et al.* [2006] suggested that the period and the wavelength of LSTIDs should be dependent on a priori condition of the source in the auroral region. Valladares *et al.* [2009] attributed the difference on auroral currents between the NH and SH polar regions. In order to investigate whether the auroral current activity in NH and SH was different or not in the present case, we show H component of the geomagnetic field in the northern and southern auroral regions in Figure 4a and the differences between the two components in Figure 4b. Both the magnetometer sites are located under auroral oval at conjugate points at Syowa (69°S , 39.6°E) and Husafell (64.7°N , 21.0°W). Some changes happened in terms of ΔH during the period of 13:00–19:00 UT, indicating that the auroral current activities were not symmetric in the NH and SH polar regions. For reference, the events SH1/NH1, SH2, SH3, NH2, and SH4/NH3 are marked in Figure 4a. It is evident that each wave event corresponds to a sudden increase/decrease of the auroral current. Further, the ΔH shown in Figure 4b indicates that there are differences between the auroral currents in NH and SH during the wave events SH1, NH1, SH3, and NH2, showing that they originate at different times and propagation conditions. This might explain why we observed different LSTID propagation in the NH and SH during the first stage of the magnetic storm, around 14:00–19:00 UT.

4.1. Phase Velocity

Comparing the phase velocity between SH and NH events, there is no significant difference in the phase speed between them for the SH1, NH1, SH3, and NH2 events. However, there is a large difference of the phase speed around 700 m/s between the SH4 and NH3 as mentioned in the previous section. This could be due to differences in the output energy at the NH and SH auroral regions which affect the LSTID propagation phase velocity. Besides, there might be an ion-drag effect and wave energy dissipation during the movement of LSTID from the auroral to low-latitude regions. In this regard, Tsugawa *et al.* [2003] suggested that the ion-drag is a main dissipation process of LSTIDs. Song *et al.* [2012] reported that the LSTIDs damping rate is higher during daytime than at nighttime. In the SH4 and NH3 wave event at 23:00 UT the SH time zone was changing from evening to night, whereas the NH zone was still in daytime. Therefore, it could be that SH4 could reach low-latitude region with a higher phase velocity because of the reduced dissipation process.

4.2. Propagation Direction

All LSTID wave events observed during the geomagnetic storm in SH showed different propagation directions, as presented in Table 1. The propagation direction of NH wave events was only to the

Table 1. LSTID Wave Parameters in SH and NH

Event	Hemisphere	Hour (UT)	Wavelength (km)	Phase Velocity (m/s)	Propagation Direction (deg)
NH1	North	14:00	1141 ± 166	476 ± 69	180–225
SH1	South	14:30	1030 ± 122	741 ± 70	0–45
SH2	South	16:00	1587 ± 265	529 ± 88	0–45
NH2	North	18:00	1050 ± 140	611 ± 69	180–225
SH3	South	18:30	904 ± 94	565 ± 74	0–45
NH3	North	23:00	785 ± 159	291 ± 59	180–225
SH4	South	23:00	1800 ± 110	1070 ± 84	270–315

southwest. On the other hand, the propagation direction of SH wave events changed from northeast during 14:00 and 19:00 UT (daytime) to northwest at 23:00 UT (nighttime). It means that the propagation direction in the NH and SH zone is asymmetric during the period of 14:00–19:00 UT and symmetric at 23:00 UT.

Previous studies reported that the propagation direction of LSTIDs in NH is normally southwest [Afraimovich et al., 2004; Afraimovich and Voeykov, 2004; Tsugawa et al., 2004; Ding et al., 2008, Valladares et al., 2009; Song et al., 2012]. A few observations carried out in SH reported the propagation direction to the northwest [Pradipta et al., 2016]. In the present work, we observed two different propagation directions, northeast and northwest. Ding et al. [2008] and Song et al. [2012] explained that the southwestward propagation in NH is related to the Coriolis force, not affected by the geomagnetic declination. The northwestward propagation of the wave SH4 could be explained by the Coriolis effect. On the other hand, the northeastward propagation of the waves SH1, SH2, and SH3 cannot be explained by the same way. Another mechanism should be considered to explain the propagation direction of northeast.

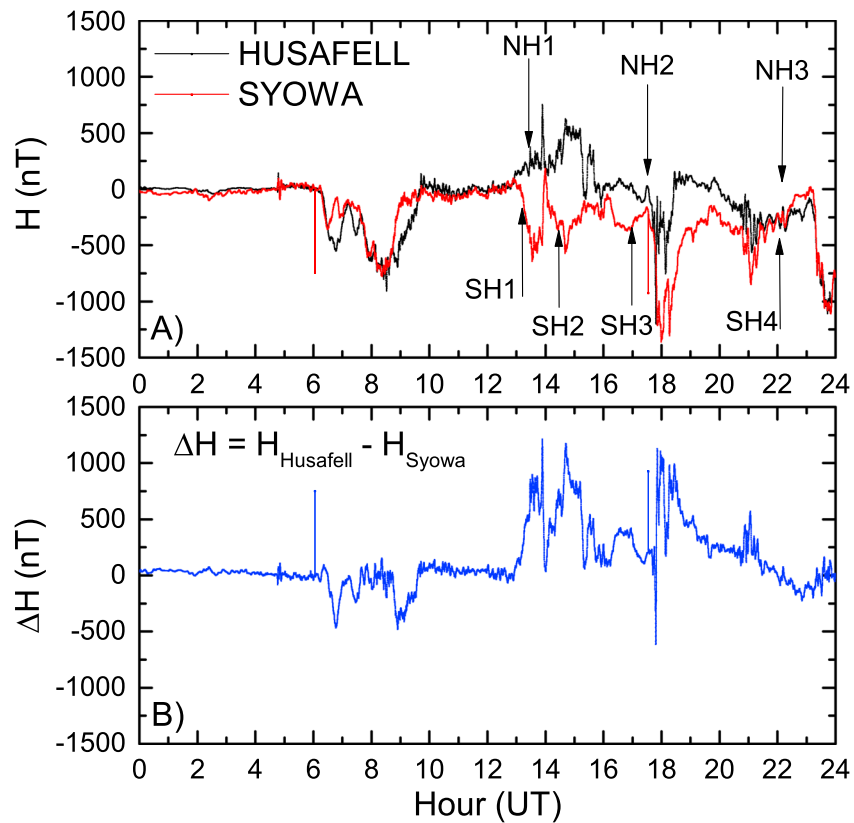


Figure 4. (a) The geomagnetic field horizontal (H) component along the northern (Husafell) and southern (Syowa) auroral regions on 17 March 2015. (b) The difference between Husafell and Syowa H components of geomagnetic field. The vertical arrows indicate the hour when LSTIDs were launched at auroral oval, considering the distance between auroral oval and 35°S in SH to be ~3000 km and at ~50°N in NH to be ~1000 km.

Several authors [e.g., Østgaard *et al.*, 2004; Laundal and Østgaard, 2009; Crowley *et al.*, 2010; Förster *et al.*, 2011; Mannucci *et al.*, 2014] have shown that the direction and magnitude of interplanetary magnetic field component (B_y) plays an important role in the development and intensity of the ionospheric storm; i.e., it modifies the ionospheric convection pattern and leads to a hemispheric asymmetry in the region 1 field-aligned currents (FACs). Recently, Astafyeva *et al.* [2015] concluded that the variation of the interplanetary magnetic field (positive B_y and negative B_z) during the main phase of the St. Patrick's storm (until 22:45 UT) generated an asymmetry in both hemispheres, producing stronger effects in the SH, especially in the American sector. As shown in Figure 4, the auroral currents were asymmetric between NH and SH. Therefore, it could be inferred that the asymmetry at auroral region might have affected the propagation direction of LSTIDs and their respective phase velocity. Further observational evidence and simulations would be necessary to explain the observations.

5. Conclusions

During the geomagnetic storm that occurred on 17 March 2015, several LSTID wave events were observed in the American sector, three at 14:00–19:00 UT (dayside) and the other at 23:00 UT (eveningside in SH and dayside in NH). The first group of LSTIDs observed at 14:00–19:00 UT, propagated toward the southwest in NH and north-northeast in SH, showing an asymmetric propagation direction against the geographic equator. The second one at 23:00 UT propagated southwestward in NH and northwestward in SH, showed a symmetric form. The observed symmetric propagation form of LSTID could be due to the symmetry of the auroral current activity. On the other hand, observed asymmetric propagation form suggests asymmetry of the auroral current activity between the northern and southern polar regions.

Acknowledgments

The GPS data used in this study were provided via the FTP servers of RBMC, RAMSAC, CORS, SOPAC, IGS, and UNAVCO. The GPS data collection and processing of CORS, SOPAC, IGS, and UNAVCO were performed with the NICT Science Cloud. The authors thank to T. Nakamura and A. Kadokura of National Institute of Polar Research (NIPR) who provided the magnetometer data at Syowa and Husafell stations. The present work was supported by Conselho Nacional de Desenvolvimento Científico e Tecnológico (CNPq) under the process 161894/2015-1, 310926/2014-9, 305461/2015-0, 141823/2016-0, and 438691/2016-4; Coordenação de Aperfeiçoamento de Pessoal de Nível Superior (CAPES) under process BEX4488/14-8; and JSPS KAKENHI under process JP 15H05815 and JP 16H06286 grants.

References

- Afraimovich, E. L., and S. V. Voeykov (2004), Experimental evidence of the existence of a solitary internal gravity wave in the Earth's atmosphere during a strong magnetic storm, *Dokl. Earth Sci.*, *399*, 683–686.
- Afraimovich, E. L., E. A. Kosogorov, L. A. Leonovich, K. S. Palamartchouk, N. P. Perevalova, and O. M. Pirog (2000), Determining parameters of large-scale traveling ionospheric disturbances of auroral origin using GPS-arrays, *J. Atmos. Sol. Terr. Phys.*, *62*, 553–565.
- Afraimovich, E. L., E. I. Astafyeva, and S. V. Voeykov (2006), Generation of ionospheric irregularities under condition of solitary internal gravitational wave propagation during the major magnetic storm of 29–31.10.2003, *Radiophys. Quantum Electr.*, *49*, 89–104.
- Afraimovich, E. L., et al. (2004), Detection of traveling ionospheric disturbances from the data of simultaneous measurements of the electron concentration, total electron content, and Doppler frequency shift at the ISTP radiophysical complex, *Geomagn. Aeron.*, *44*(N4), 463–475.
- Astafyeva, E., I. Zakharenkova, and M. Förster (2015), Ionospheric response to the 2015 St. Patrick's day storm: A global multi-instrumental overview, *J. Geophys. Res. Space Physics*, *120*, 9023–9037, doi:10.1002/2015JA021629.
- Crowley, G., D. J. Knipp, K. A. Drake, J. Lei, E. Sutton, and H. Lühr (2010), Thermospheric density enhancements in the dayside cusp region during strong B_y conditions, *Geophys. Res. Lett.*, *37*, L07110, doi:10.1029/2009GL042143.
- Ding, F., W. Wan, B. Ning, and M. Wang (2007), Large-scale traveling ionospheric disturbances observed by GPS total electron content during the magnetic storm of 29–30 October 2003, *J. Geophys. Res.*, *112*, A06309, doi:10.1029/2006JA012013.
- Ding, F., W. Wan, L. Liu, E. L. Afraimovich, S. V. Voeykov, and N. P. Perevalova (2008), A statistical study of large-scale traveling ionospheric disturbances observed by GPS TEC during major magnetic storms over the years 2003–2005, *J. Geophys. Res.*, *113*, A00A01, doi:10.1029/2008JA013037.
- Förster, M., S. E. Haaland, and E. Doornbos (2011), Thermospheric vorticity at high geomagnetic latitudes from CHAMP data and its IMF dependence, *Ann. Geophys.*, *29*(1), 181–186.
- Hocke, K., and K. Schlegel (1996), A review of atmospheric gravity waves and travelling ionospheric disturbances: 1982–1995, *Ann. Geophys.*, *14*, 917–940, doi:10.1007/s00585-996-0917-6.
- Hunsucker, R. D. (1982), Atmospheric gravity waves generated in the high-latitude ionosphere: A review, *Rev. Geophys.*, *20*, 293–315, doi:10.1029/RG020i002p00293.
- Laundal, K. M., and N. Østgaard (2009), Asymmetric auroral intensities in the Earth's Northern and Southern Hemispheres, *Nature*, *460*, 491–493, doi:10.1038/nature08154.
- Mannucci, A. J., B. A. Iijima, U. J. Lindqwister, X. Pi, L. Sparks, and B. D. Wilson (1999), GPS and ionosphere, in *Review of Radio Science 1996–1999*, edited by W. R. Stone, pp. 625–665, Int. Union of Radio Sci, Ghent, Belgium.
- Mannucci, A. J., G. Crowley, B. T. Tsurutani, O. P. Verkhoglyadova, A. Komjathy, and P. Stephens (2014), Interplanetary magnetic field B_y control of prompt total electron content increases during superstorms, *J. Atmos. Sol. Terr. Phys.*, *115*, 7–16, doi:10.1016/j.jastp.2014.01.001.
- Narayanan, V. L., K. Shiokawa, Y. Otsuka, and S. Saito (2014), Airglow observations of nighttime medium-scale traveling ionospheric disturbances from Yonaguni: Statistical characteristics and low-latitude limit, *J. Geophys. Res. Space Physics*, *119*, 9268–9282, doi:10.1002/2014JA020368.
- Nicolls, M. J., M. C. Kelley, A. J. Coster, S. A. Gonzalez, and J. J. Makela (2004), Imaging the structure of a large-scale TID using ISR and TEC data, *Geophys. Res. Lett.*, *31*, L09812, doi:10.1029/2004GL019797.
- Østgaard, N., S. B. Mende, H. U. Frey, T. J. Immel, L. A. Frank, J. B. Sigwarth, and T. J. Stubbs (2004), Interplanetary magnetic field control of the location of substorm onset and auroral features in the conjugate hemispheres, *J. Geophys. Res.*, *109*, A07204, doi:10.1029/2003JA010370.
- Pradipta, R., C. E. Valladares, B. A. Carter, and P. H. Doherty (2016), Interhemispheric propagation and interactions of auroral traveling ionospheric disturbances near the equator, *J. Geophys. Res. Space Physics*, *121*, 2462–2474, doi:10.1002/2015JA022043.
- Saito, A., S. Fukao, and S. Miyazaki (1998), High resolution mapping of TEC perturbations with the GSI GPS network over Japan, *Geophys. Res. Lett.*, *25*, 3079–3082, doi:10.1029/98GL52361.

- Saito, S., M. Yamamoto, H. Hashiguchi, A. Maegawa, and A. Saito (2007), Observational evidence of coupling between quasi-periodic echoes and medium scale traveling ionospheric disturbances, *Ann. Geophys.*, *25*, 2185–2194, doi:10.5194/angeo-25-2185-2007.
- Shiokawa, K., et al. (2005), Geomagnetic conjugate observation of nighttime medium-scale and large-scale traveling ionospheric disturbances: FRONT3 campaign, *J. Geophys. Res.*, *110*, A05303, doi:10.1029/2004JA010845.
- Sobral, J. H. A., et al. (2001), Thermospheric *F* region travelling disturbances detected at low latitude by an OI 630 nm digital imager system, *Adv. Space Res.*, *27*, 1201–1206, doi:10.1016/S0273-1177(01)00198-3.
- Song, Q., F. Ding, W. Wan, B. Ning, and L. Liu (2012), Global propagation features of large-scale traveling ionospheric disturbances during the magnetic storm of 7–10 November 2004, *Ann. Geophys.*, *30*, 683–694, doi:10.5194/angeo-30-683-2012.
- Takahashi, H., et al. (2016), Ionospheric TEC weather map over South America, *Space Weather*, *14*, 937–949, doi:10.1002/2016SW001474.
- Taylor, M. J., P.-D. Pautet, A. F. Medeiros, R. Buriti, J. Fechine, D. C. Fritts, S. L. Vadas, H. Takahashi, and F. T. São Sabbas (2009), Characteristics of mesospheric gravity waves near the magnetic equator, Brazil, during the SpreadFEx campaign, *Ann. Geophys.*, *27*, 461–472, doi:10.5194/angeo-27-461-2009.
- Tsugawa, T., A. Saito, Y. Otsuka, and M. Yamamoto (2003), Damping of large-scale traveling ionospheric disturbances detected with GPS networks during the geomagnetic storm, *J. Geophys. Res.*, *108*(A3), 1127, doi:10.1029/2002JA009433.
- Tsugawa, T., A. Saito, and Y. Otsuka (2004), A statistical study of largescale traveling ionospheric disturbances using the GPS network in Japan, *J. Geophys. Res.*, *109*, A06302, doi:10.1029/2003JA010302.
- Tsugawa, T., K. Shiokawa, Y. Otsuka, T. Ogawa, A. Saito, and M. Nishioka (2006), Geomagnetic conjugate observations of large-scale traveling ionospheric disturbances using GPS networks in Japan and Australia, *J. Geophys. Res.*, *111*, A02302, doi:10.1029/2005JA011300.
- Tsugawa, T., Y. Otsuka, A. J. Coster, and A. Saito (2007), Medium-scale traveling ionospheric disturbances detected with dense and wide TEC maps over North America, *Geophys. Res. Lett.*, *34*, L22101, doi:10.1029/2007GL031663.
- Valladares, C. E., J. Villalobos, M. A. Hei, R. Sheehan, S. Basu, E. MacKenzie, P. H. Doherty, and V. H. Rios (2009), Simultaneous observation of travelling ionospheric disturbances in the Northern and Southern Hemispheres, *Ann. Geophys.*, *27*, 1501–1508, doi:10.5194/angeo-27-1501-2009.